Source-space Waveform Reconstruction for Coherent Brain Signals

Kiwoong Kim[*] [†]
[*]Korea Research Institute of Standards and Science (KRISS), Daejeon 305-340, Republic of KOREA
[†]E-mail: kwkim@kriss.re.kr Tel: +82-42-868-5676

***Abstract*— In electro- or magneto-encephalographic muliti-channel measurements, signal-source space analysis is inevitable for brain functional-connectivity studies since the detector-space signals are mixed up with signal sources and they give fake correlation. However, many methods for the reconstruction of the source waveform such as beamforming techniques and MUSIC suffer from inaccurate source separation caused by power leaking between correlated sources. Such power leaking can be circumvented by suppressing correlated sources with linear constraints. In this study, I demonstrate such correlated source suppression can be used to preserve local phase information and the reconstructed source waveforms provide more accurate phase information for brain functional coherence and directivity analysis.**

I. INTRODUCTION

Many brain researchers have been getting to be interested in more and more complex brain functions as well as primary functional mapping like visual, auditory, and somatosensory responses. A design of an event-related potential (ERP) paradigm for such a higher-order cognition (HOC) study is quite tricky. Therefore, changes in spontaneous neuroelectric oscillation have widely been analyzed for such tasks. In some induced HOC responses, the latency or delay after stimulus is different individual by individual. Thus, continuous recordings have typically been conducted rather than stimulus-triggered measurements.

Meanwhile, functional connectivity and directivity studies are one of the mainstreams in the brain researches. Some of the studies are conducted by fMRI, but those researches have limitation since the time-resolution of the BOLD effect in fMRI is too low to analyze a high speed activity in a brain. Another option is to measure neuroelectric oscillation by using electroencephalography (EEG) or magnetoencephalography (MEG) and to analyze the phase information of the oscillation at different sites. In the past, most of the connectivity studies dealing with correlation and phase information among different sites were based on the sensor space analysis, i.e. a direct analysis of measured potentials at electrodes or measured magnetic fields with SQUID sensors. However, such sensor space analyses were proven to be meaningless in a strict sense since they can have high correlation coefficient value due to a mixing effect in a volume conductor media even for non-synchronized sources [1]. Hence a source space analysis is required to find out the brain functional connectivity and we need to reconstruct the neuroelectric oscillation at the source position from the measured multichannel signals.

To localize and reconstruct decorrelated sources from the continuous recordings of multichannel measurements like EEG and MEG, spatial filtering techniques could be adopted generally [2-3]. The connectivity in the neural network is believed to play an important role in HOC processes and the connected sources in different positions are assumed to be activating coherently. The coherent sources would be measured as mixed waveforms with a sensor array and usual principal component analysis or independent component analysis cannot decompose the recorded signal into the correct sources, hence informative localization fails in EEG or MEG [4]. The power leakage interference between correlated sources in the minimum variance spatial filtering (MVSF) is a well-known main reason for the failure in the source localization of MVSF, and the leakage can be improved by applying source suppression with a linearly-constrained (LC) MVSF. [2]. One can easily expect that the power leakage can affect not only localization results but also reconstruction results of the source waveform. Especially, the mixing-up of two coherent waves with different phases will ruin the phase information one another, which would result in a failure of directivity estimation. In this study, by conducting MEG simulation, I demonstrate the performance of LCMVSF to sustain phase information of coherent sources as well as the localization performance. Also I show the performance depends on the suppression area because the linear-constraints tend to have a more overlap with the source lead field, i.e. linearly dependent as the area get increased.

II. METHODS

A. *Head Conductor Model and MEG Sensor Arrangement*

In the following simulation, we assumed to use an MEG system for measuring the coherence sources since the magnetic field is not affected from surrounding mediums like skull and skin after its generation from the post-synaptic neuronal primary currents, which is advantageous to rigorous localization and reconstruction of the correlated sources. The simulated MEG measurement is based on KRISSMEG system (Korea Research Institute of Standards and Science, Daejeon, Korea). The system consists of 152 double relaxation oscillation SQUID sensors distributed on a helmet surface surrounding a human head (Fig. 1). The pick-up coil type is

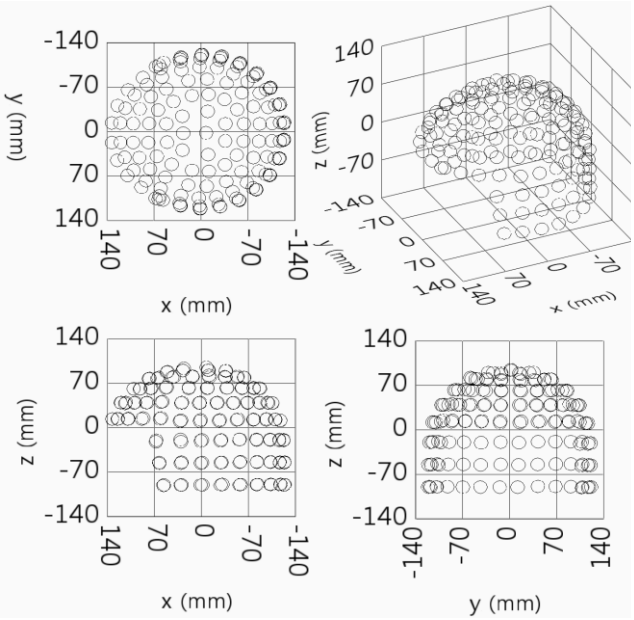

Fig. 1 The SQUID sensor arrangement of KRISSMEG system. The center of the spherically-symmetric head conductor model is placed at the origin.

the first-order gradiometer of 40-mm baseline. The head conductor model is the spherically symmetric model [5] centered at the origin of Fig. 1. The noise of each sensor was approximated to 10 fT_{rms}/cm assuming 100-Hz bandwidth and 4 fT/√Hz. The sampling rate of the system is set to 500Hz.

B. Linearly-constrained Minimum Variance Spatial Filter

In general, we can denote the *n*-channel measured magnetic field as a linear combination of lead-field vector projected from every current dipole moment components in the source space. As an inverse procedure, we can estimate the source dipole vectors by multiplying a weight vector by the measured magnetic fields. In that case, we can regard the weight vector as a spatial filter projecting a source component from the measured fields. Basically, the MVSF is to find a weight vector which minimizes the output source power under the constraint that the dot product of weight vector and lead-field vector becomes identity only when their source positions are the same; if not, the product should be zero. For sources of no correlation, MVSF has a good performance in localizing sources and in reconstructing the waveform in the source position. However, unfortunately, neuronal activities are strongly-correlated in most cases. The easiest idea to circumvent this problem is simply to estimate sources of interest after separating all the other correlated sources. Thus, we need to use more strong constraints other than the previous constraint at the one source position of interest. These constraints can linearly be added in a manner of extended lead field vectors at the suppressing points.

In order to add the constraints, we define a region where to suppress the sources correlated to the source of interest. Generally, the region consists of a cluster of positions. Let the position vectors, $r_{(1)},\ldots,r_{(Nc)}$, denote the locations of the voxels within the region, where N_c is the total number of voxels within the cluster. An $n\times 3N_c$ constraint matrix $\mathbf{L_c}$ is defined such that,

$$\mathbf{L}_c = \left[L(r_{(1)}),\ldots, L(r_{(N_c)}) \right], \tag{1}$$

where $L(r)$ is the $n\times 3$ lead-field matrix, $L(r)$ is defined such that

$$L(r) = \left[l_c^{(x)}(r), l_c^{(y)}(r), l_c^{(z)}(r) \right], \tag{2}$$

where $l_c^{(x)}(r)$, $l_c^{(y)}(r)$, and $l_c^{(z)}(r)$ are the $n\times 1$ normalized lead-field column unit vectors generated by the three orthogonal components of a current dipole at the position. Then the cluster suppressed source power located at $r=(x,y,z)^{\mathrm{T}}$ is defined as

$$\hat{P}_c(r) \equiv tr\left\{ \left[\tilde{\mathbf{L}}^{\mathrm{T}}(r)(\mathbf{C}+\varepsilon\mathbf{I})^{-1}\tilde{\mathbf{L}}(r) \right]^{-1} \right\}, \tag{3}$$

Where

$$\tilde{\mathbf{L}}(r) = \left[\frac{l^{(x)}(r)}{\left\| l^{(x)}(r) \right\|}, \frac{l^{(y)}(r)}{\left\| l^{(y)}(r) \right\|}, \frac{l^{(z)}(r)}{\left\| l^{(z)}(r) \right\|}, \mathbf{L_c} \right], \tag{4}$$

C is the covariance matrix of the measurement, ε is the regularization parameter and $\|\cdot\|$ is the Euclidean norm. The size of the suppressing cluster can vary according to the measurement and analysis conditions. If the number of suppression voxels is much smaller than the number of channel, Eq. (3) could give a reasonable result. However, if the number of the voxels exceeds the rank, we need to compress the matrix $\mathbf{L_c}$ by applying singular-value decomposition or eigen-space reduction.

In this study, we tested two ultimate conditions; one is point suppression and the other is a cluster suppression to suppress whole sources of either hemisphere. In the large cluster separation condition described in the following section, the number of constraint vectors is 3 x 680 points and 95% of the lead-field feature can be expressed by 7-8 eigenvectors. Hence, the number of column in the constraint lead-field is about 10.

The wave form can be reconstructed by multiplying the weight vector by the measured time trace signals. The weight vector would be expressed like the following.

$$w(r) \equiv \left[\tilde{\mathbf{L}}^{\mathrm{T}}(r)(\mathbf{C}+\varepsilon\mathbf{I})^{-1}\tilde{\mathbf{L}}(r) \right]^{-1}\tilde{\mathbf{L}}^{\mathrm{T}}(r)(\mathbf{C}+\varepsilon\mathbf{I})^{-1}s, \tag{5}$$

TABLE I
SOURCE CURRENT DIPOLE NUMBERING, POSITION, AND ORIENTATION

No.	Source Current Dipole Features		
	Position Coordinate [mm] (x, y, z)	Strength [nA·m]	Orientation (x, y, z)
1	Left Hemisphere (-10, 30, 50)	100	(0, 1/√2, 1/√2)
2	Right Hemisphere (10, -30, 50)	100	(0, -1/√2, 1/√2)

where s is a unit vector selecting one of the components of the lead-field vector of interest.

III. NUMERICAL SIMULATIONS

A. Coherent Sources

Two coherent current dipoles are located at (-10 mm, 30 mm, 50 mm) and (10 mm, -30 mm, 50 mm), which are corresponding to left- and right-hemisphere of a human brain, respectively. The other features of the dipole sources are specified in Table I. Sinusoidal excitation is applied on each position. The frequency of the excitation is 10 Hz, which is equal to both sources to conserve the coherency between the two sources. The acquisition time is 2s, which is corresponding to 1000 sample points. Therefore, more than six-times longer than the number of channels hence the covariance matrix estimated from the time traces satisfies the rank condition. The phase of dipole number one is fixed to 0 deg and the phase of dipole number two varies from 0 to 180 deg. For the assessment of the waveform reconstruction, the source at the position of dipole number one is going to be calculated and estimated.

B. Source Space

For the assessment of the localization, a three-dimensional mesh is introduced. The mesh is a rectangular parallelepiped covering the two dipole sources. The coordinates of the covering volume span from -40 (mm) to 40 (mm) for x- and y-axis, and from 40 (mm) to 60 (mm) for z-axis, respectively. All those mesh points are located inside a sphere of 85 mm radius. The scanning interval is 5 mm, which is small enough for the point-spread sensitivity of the lead field of the spatial filter at the depth of the source locations. The total number of the scan points is 1445.

The source space is divided into two portions to test the cluster source suppression. In this study, one portion is the left-hemisphere ($y>0$) and the right-hemisphere ($y<0$). The one portion contains 680 source points and it exceeds the number of sensors. Thus, the suppression constraints for each individual point make a singular matrix caused by a rank problem. Therefore, as described in the method section, one portion should collectively be approximated by high singular valued eigen-leadfield vectors.

.

IV. RESULTS AND DISCUSSION

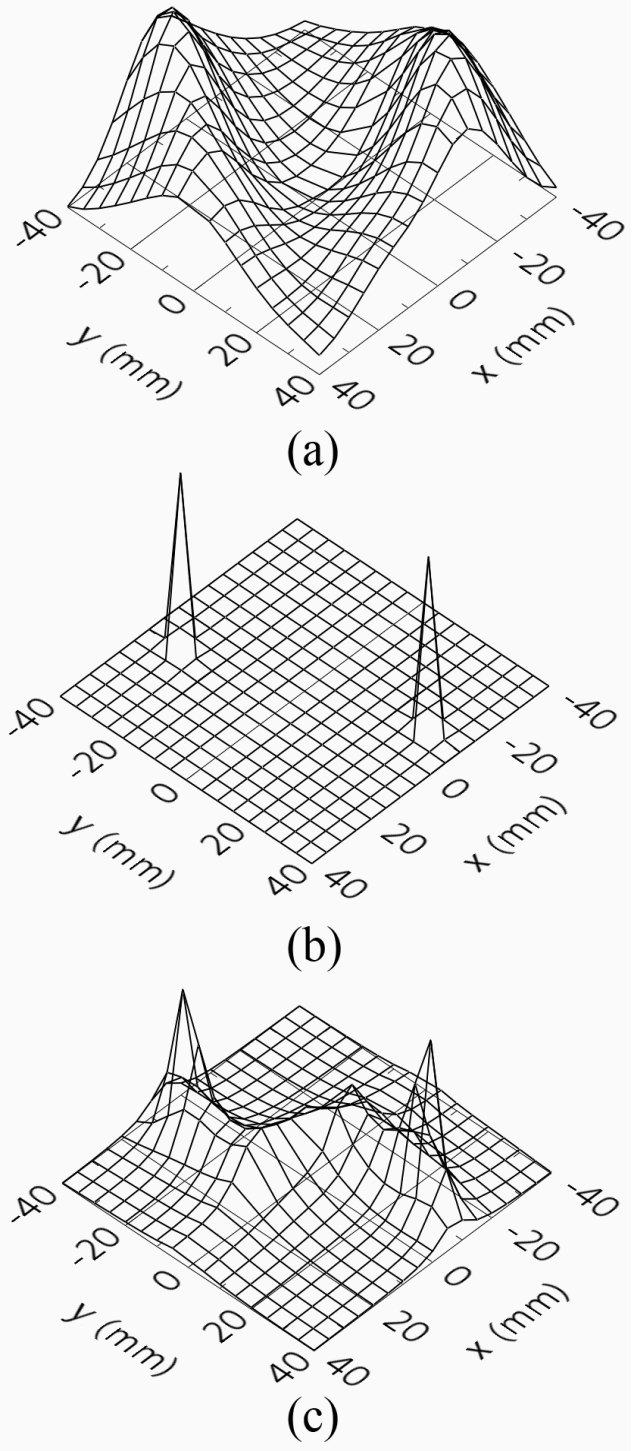

Fig. 2 Performance of source localization for coherent sources with (a) no correlated source suppression, (b) point suppression, and (c) cluster suppression. In this estimation, two sources were oscillating with an exactly same phase. The figures show the source power estimated by spatial filtering. For all the cases, the estimation plane was placed at z=50.

The performance of the completely-correlated source localization results are shown in Fig. 2. All the pictures indicate the source power on the source space plane at z=50

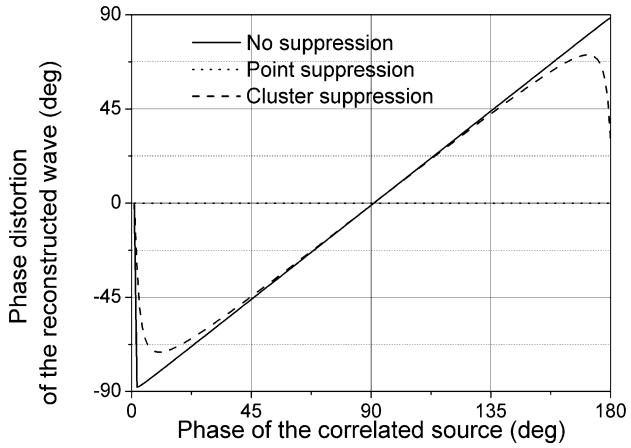

Fig. 3 Phase distortion by interference of a coherent source. The figure indicates the degree of the phase error in the reconstructed waveform as a function of the relative phase difference between the coherent sources.

(mm). The first figure is a result for the ordinary MVSF without an additional linear constraint. The figure implies that the power leakage between two correlated sources is too severe to localize the accurate positions of the source current dipoles. The second is the result of a case for suppressing a correlated source at the point of the location of source number two. In spite that the two sources are completely correlated with each other, the point suppression gave an exact localization result. The last figure is the result of cluster suppression. As described in the previous section, we adopt to use a limit-case clustering, i.e. suppression of whole sources in the contra-lateral hemisphere. Although there is some artifact due to a constraint overlap with the lead-field, the local maxima of the estimated source power are clearly indicating the exact source positions.

Fig. 3 shows the phase of reconstructed source at the position of dipole number one as a function of the phase of the source dipole number two. The solid, dotted, and dashed lines in Fig. 3 are for unsuppressed sources, cluster-suppressed sources, and point-suppressed sources, respectively. While the source waveform reconstruction under point suppression was not affected by the relative phase of another coherent source, the other two cases showed severe interference between the coherent sources depending on the relative phase.

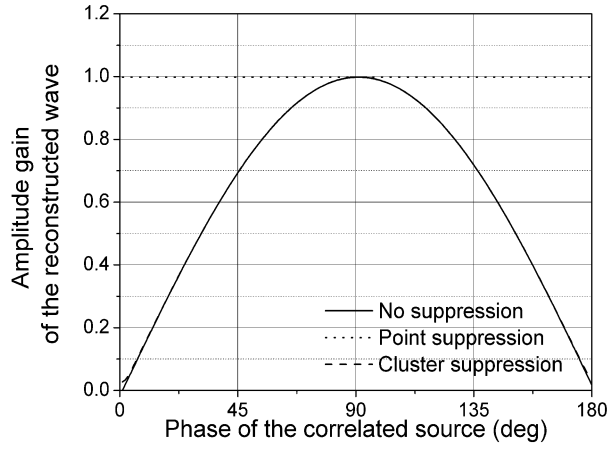

Fig. 4 Power leakage by interference of a coherent source. The figure indicates the amplitude reduction in the reconstructed waveform as a function of the relative phase difference between the coherent sources.

In the same situation, changes of the reconstructed waveform amplitude depending on the relative phase of the other correlated source were depicted in Fig. 4. The figure implies the point suppression can perfectly prevent the power leakage between coherent sources regardless of the relative phase. As a matter of course, we can see there is no distortion at the 90-deg relative phase difference since 90-deg difference gives zero correlation coefficient even for the coherent sources oscillating with a same frequency.

Although the point suppression was most effective to localize and reconstruct the coherent sources in the simulation, in general case, it is hard to expect to know where to place the point suppression constraint because we are not sure of the exact location of the correlated source. In such cases, an iterative application of LC-MVSF with decreasing the region of suppression from a wide range to a focused point could be a solution. In addition, we need to estimate a reasonable final size of the suppressing cluster during the iteration by monitoring the phase change of the reconstructed waveform.

Another possible problem exists when there are two closely located coherent sources. In those situations, we cannot guarantee the independency between the two lead field vectors at each source location. Therefore, the degree of the suppression accuracy depends on the point-spread sensitivity function of the sensor system at the source positions.

REFERENCES

[1] P. Tass, et al., "Detection of n:m Phase Locking from Noisy Data: Application to Magnetoencephalography," *Phys. Rev. Lett.* , Vol. 81, pp. 3291-3294, 1998.

[2] B. D. Van Veen, W. van Drongelen, M. Yuchtman, A. Suzuki, "Localization of brain electrical activity via linearly constrained minimum variance spatial filtering ," *IEEE Trans. Biomed. Eng.*, Vol. 44(9), pp. 867-880, 1997.

[3] K. Sekihara, S. S. Nagarajan, D. Poeppel, and A. Marantz, "Performance of an MEG Adaptive-Beamformer Technique in the Presence of Correlated Neural Activities: Effects on Signal Intensity and Time-Course Estimates," *IEEE Trans. Biomed. Eng.*, Vol. 49(12), DECEMBER 2002.

[4] K. Kim, Y. H. Lee, H. Kwon, J. H. Bae, "Independent component analysis for synthetic aperture magnetometry in magnetocardiography," *Comput. Biol. Med.*, 36(3), pp. 253-261, 2006.

[5] J Sarvas, "Basic mathematical and electromagnetic concepts of the biomagnetic inverse problem," *Phys. Med. Biol.* Vol. 32, pp. 11-22, 1987